Calculation of the Distributions of Magnetic Fields used in Rotary-saturation Experiments

Yoshinori MANMOTO and Shigeaki TAKASE*

Department of Electronic Science,
Okayama University of Science, Ridai-cho 1-1 Okayama 700, Japan
**Ayumi Industries, Ltd, Himeji 671-02, Japan*

(Received September 25, 1981)

In order to interpret the disagreement between the experimental results and the theory in the rotary-saturation study, the distributions of the magnetic-field intensities are calculated. It is found that this discrepancy is considerably reduced by using these distributions, but it is not sufficient to consider only these distributions. It is necessary to consider another physical factors for the correction of this discrepancy. The actual calculation is made over 435600 sites in the sample by using numerical integrals by computor.

1. Introduction

Nuclear Magnetic Resonance (NMR) is a very useful method to obtain the informations at atomic and molecular levels in materials. Moreover, in nuclear magnetic resonance there are phenomena Redfield[1] called rotary saturation and this saturation technique is also useful.

In the past, the study of multiple-quantum transitions (m.q.t.) was carried out by atomic and molecular beem methods[2),3)], or a similar type to these methods.[4)] However, these methods can not be applied to observing m. q. t. signals in solids. On the other hand, rotary-saturation method enable us to observe m.q.t. signals in solids, not to speak of gases and liquids.[5)]

We reported the study of m.q.t. of Na nuclei in a NaCl single crystal by this technique and deduced the formulas for analyzing multiple-quantum processes.[6)] However, in that paper the experimental results can not be explained throughly by those formulas. Though multiple-quantum processes of F nuclei in a CaF_2 single crystal are under studying, but also in this cace the observed values can not agree with caculated values by our formulas.

In this paper, we supposed the inhomogeneities of the coils used in our experimental apparatus as one of the causes for this disagreement and estimated the effect of these inhomogeneities on the results of m. q. t. obtained in our rotary-saturation experiment. Rotary-saturation apparatus needs to an audio-frequency channel other than a radio-frequency channel contrast to standard nuclear-resonance apparatus. Our experiments have been performed using ordinary pulsed NMR apparatus with an audio channel. In order to estimate the effect of inhomogeneities, the distributions of the strengths of both magnetic fields—radio-frequency field (H_1) and audio-frequency field (Ha)—were calculated by computor. In numerical calculation Hewlett-Packard 9825B desktop computor was used. Romberg sterometry was utilized in numerical integration.

2. Calculation of the Distribution of the Magnetic Field Strength

The arrangment of the two different type Helmholtz coils and sample used in our rotary-saturation experiment is shown in Fig. 1. Their dimensions are also shown in this figure. (in millimeter units) The inner cylindrical and outer circular Helmholtz pairs are those to generate *rf* field H_1 and *af* field H_a respectively. Receiver coil is put inside and perpendicular to both coils. Sample is placed inside these three coils. Electromagnet is coaxial with H_a coils and placed outside these three coils.

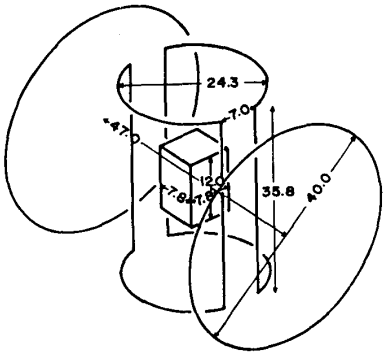

Fig. 1 Schematic diagram of the coil geometry at the sample.

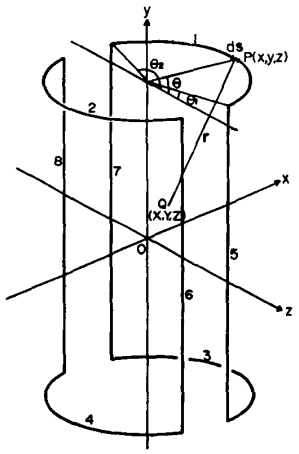

Fig. 2 Specifications for the cylindrical Helmholtz coils and the coordinate system.

2. 1 Calculation of H_1 Field

The various quantities used in calculation are defined in Fig. 2 and for convenience the coils are divided into eight sections. The vector potential A produced by the electric current J which flows through the very small amount ds of a wire

at the point P on the circular arc (1) is

$$\boldsymbol{A}=\frac{\mu_0 N}{4\pi}\int\frac{J}{r}d\boldsymbol{s}, \tag{1}$$

where μ_0 is magnetic permeability in free space, N is number of turns in the coil. $\boldsymbol{r}$ is a vector directed from point P to Q and its magnitude is

$$r=[(X-x)^2+(Y-y)^2+(Z-z)^2]^{1/2}. \tag{2}$$

The relation between a vector potential $\boldsymbol{A}$ and the corresponding magnetic field $\boldsymbol{H}_1$ is

$$\boldsymbol{H}_1=\frac{1}{\mu_0}\text{rot}\,\boldsymbol{A}. \tag{3}$$

Substituting eq. (1) into (3),

$$\boldsymbol{H}_1=\frac{NJ}{4\pi}\int \frac{\boldsymbol{i}[-(Y-y)dz+(Z-z)dy]+\boldsymbol{j}[-(Z-z)dx+(X-x)dz]+\boldsymbol{k}[-(X-x)dy+(Y-y)dx]}{[(X-x)^2+(Y-y)^2+(Z-z)^2]^{3/2}}, \tag{4}$$

where $\boldsymbol{i}$, $\boldsymbol{j}$ and $\boldsymbol{k}$ are unit vectors along x, y and z axes respectively. As is evident from Fig. 2,

$$x=a\sin\theta,\quad y=b,\quad z=a\cos\theta, \tag{5}$$

where a is the radius of the four circular arcs, b is the half length of straight line part of these coils. Using eq. (5), the magnetic field $\boldsymbol{H}_{11}$ produced by the current through the arc wire 1 can be rewritten

$$\boldsymbol{H}_{11}=\frac{NJa}{4\pi}\int_{\theta_2}^{\theta_1}\frac{\boldsymbol{i}(Y-b)\sin\theta+\boldsymbol{j}(-X\sin\theta-Z\cos\theta+a)+\boldsymbol{k}(Y-b)\cos\theta}{[(X-a\sin\theta)^2+(Y-b)^2+(Z-a\cos\theta)^2]^{3/2}}d\theta. \tag{6a}$$

In much the same way as the derivation of $\boldsymbol{H}_{11}$ we can deduce the contributions of the currents through the other three arc wires to the magnetic field strengths $\boldsymbol{H}_{12}$, $\boldsymbol{H}_{13}$, $\boldsymbol{H}_{14}$ at the point (X, Y, Z).

$$\boldsymbol{H}_{12}=\frac{NJa}{4\pi}\int_{\theta_1}^{\theta_2}\frac{\boldsymbol{i}(Y-b)\sin\theta+\boldsymbol{j}(-X\sin\theta+Z\cos\theta-a)+\boldsymbol{k}(Y-b)\cos\theta}{[(X+a\sin\theta)^2+(Y-b)^2+(Z-a\cos\theta)^2]^{3/2}}d\theta. \tag{6b}$$

$$\boldsymbol{H}_{13}=\frac{NJa}{4\pi}\int_{\theta_1}^{\theta_2}\frac{\boldsymbol{i}(Y+b)\sin\theta+\boldsymbol{j}(-X\sin\theta-Z\cos\theta+a)+\boldsymbol{k}(Y+b)\cos\theta}{[(X-a\sin\theta)^2+(Y+b)^2+(Z-a\cos\theta)^2]^{3/2}}d\theta. \tag{6c}$$

$$\boldsymbol{H}_{14}=\frac{NJa}{4\pi}\int_{\theta_1}^{\theta_2}\frac{\boldsymbol{i}(Y+b)\sin\theta+\boldsymbol{j}(-X\sin\theta+Z\cos\theta-a)+\boldsymbol{k}(Y+b)\cos\theta}{[(X+a\sin\theta)^2+(Y+b)^2+(Z-a\cos\theta)^2]^{3/2}}d\theta. \tag{6d}$$

The contributions of the four straight line sections to the magnetic field strengths at the point Q can be deviated in similar way as above mentioned.

$$\boldsymbol{H}_{15}=\frac{NJa}{4\pi}\int_{-b}^{+b}\frac{\boldsymbol{i}(Z-a\cos\theta_1)-\boldsymbol{k}(X-a\sin\theta_1)}{[(X-a\sin\theta_1)^2+(Y-y)^2+(Z-a\cos\theta_1)^2]^{3/2}}dy. \tag{7a}$$

$$\boldsymbol{H}_{16}=\frac{NJa}{4\pi}\int_{-b}^{+b}\frac{\boldsymbol{i}(Z-a\cos\theta_1)-\boldsymbol{k}(X+a\sin\theta_1)}{[(X+a\sin\theta_1)^2+(Y-y)^2+(Z-a\cos\theta_1)^2]^{3/2}}dy. \tag{7b}$$

$$\boldsymbol{H}_{17}=\frac{NJa}{4\pi}\int_{-b}^{+b}\frac{\boldsymbol{i}(Z-a\cos\theta_2)-\boldsymbol{k}(X-a\sin\theta_2)}{[(X-a\sin\theta_2)^2+(Y-y)^2+(Z-a\cos\theta_2)^2]^{3/2}}dy. \tag{7c}$$

$$\boldsymbol{H}_{18}=\frac{NJa}{4\pi}\int_{-b}^{+b}\frac{\boldsymbol{i}(Z-a\cos\theta_2)-\boldsymbol{k}(X+a\sin\theta_2)}{[(X+a\sin\theta_2)^2+(Y-y)^2+(Z-a\cos\theta_2)^2]^{3/2}}dy. \tag{7d}$$

Since rf field H_1 is the sum of the x components of above eight fields,

$$H_1=\sum_{i=1}^{8}H_{1i}x \tag{8}$$

Using eqs. (6), (7) and (8), H_1-field strength at any point (X, Y, Z) in the sample can be calculated numerically by computor. In computing one eighth portion of sample is divided into 33 sections at intervals of 0.12 millimeters along positive x and z axes and into 50 sections along positive y axis at the same intervals. Therefore actual computor calculation is made at 54450 sites for one eighth of sample. As a result, we treate 435600 sites in full sample.

2. 2 Calculation of H_a Field

Since the expression of H_a field can be deduced in the similar way in the case of H_1, we describe only the final expressions of H_a-field strength.

$$\boldsymbol{H}_{a1}=\frac{NJc}{4\pi}\int_0^{2\pi}\frac{\boldsymbol{i}(Z-d)\cos\theta+\boldsymbol{j}(Y-c)\sin\theta-\boldsymbol{k}(X\cos\theta+Y\sin\theta-c)}{[(X-c\cos\theta)^2+(Y-c\sin\theta)^2+(Z-d)^2]^{3/2}}d\theta. \tag{9a}$$

$$\boldsymbol{H}_{a2}=\frac{NJc}{4\pi}\int_0^{2\pi}\frac{\boldsymbol{i}(Z+d)\cos\theta+\boldsymbol{j}(Z+d)\sin\theta-\boldsymbol{k}(X\cos\theta+Y\sin\theta-c)}{[(X-c\cos\theta)^2+(Y-c\sin\theta)^2+(Z+d)^2]^{3/2}}d\theta. \tag{9b}$$

Since H_a is the sum of z components of above two magnetic fields,

$$H_a=H_{a1z}+H_{a2z}. \tag{10}$$

Using eqs. (9) and (10), H_a-field strength at any point (X, Y, Z) in the sample can be calculated numerically by computor. In actual computaion, the way of division and the number of reference sites in the sample are the same in the case of H_1 calculation.

3. Results and Application

3. 1 Results of Calculation

Results of H_1 and H_a calculations are shown in Figs. 3 and 4 repectively. In both figures, the trasverse axis represents the magnetic field intensity at any point in the sample relative to the origin's and the longitudinal axis represents the number of sites which have the same value of relative intensity. As is obvious from Fig. 3, the number of the nuclei which experience much the same intensity of magnetic field as that at the center of the sample is most and the numbers in stronger and weeker fields decrease gradually. The maximum field which nuclei see is about 1.06 times large as the field at the center of the sample and the minimum one is about 0.93 times. The half-value width of this distribution is about 4.1 percents.

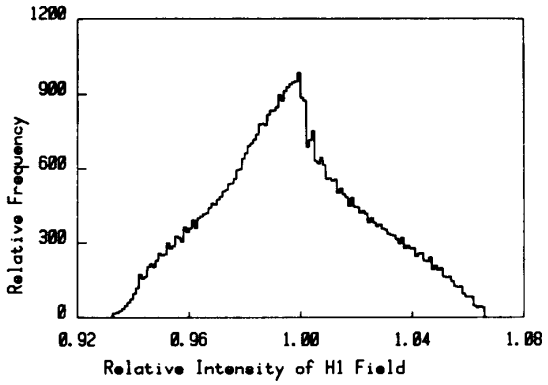

Fig. 3 Distribution of H_1 field intensity.

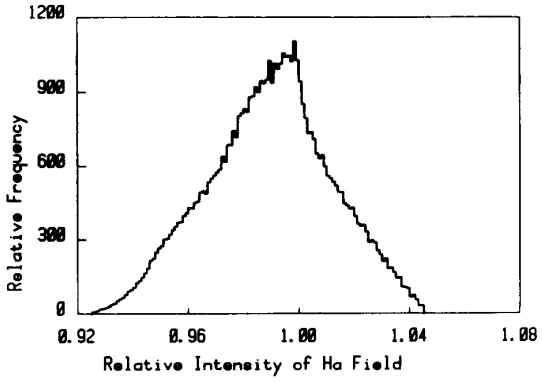

Fig. 4 Distribution of Ha field intensity.

H_a's case also shows smilar tendency as clearly from Fig. 4. The maximum and minimum fields are about 1.04 and 0.93 times large as the field at the center of the sample, respectively and the half-value width is 4.7 percents. Thus the nuclear spins at various sites in our sample experience over a wide range of H_1 and H_a-field intensities.

3. 2 Correction of the rotary-saturation results by the results of the calculation

We apply the results of the calculation in Sec. 2 to the analysis of the results obtained by our rotary-saturation experiments. An example of the cerrections is given in Fig. 5. Its horizontal axis shows H_a-pulse amplitude in terms of voltage.

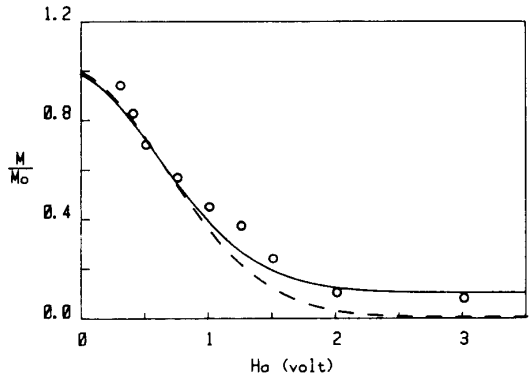

Fig. 5 The fraction of magnetization versus an audio-pulse amplitude in the rotary-saturation experiment.

Its vertical axis shows the fraction of magnetization remaining after audio pulse. The experimental points express the fraction of magnetization corresponding the first-order absorption. The solid line is that calculated by our formula in considering the distributions of the relative intensities of H_1 and H_a field. On the other hand, the dashed line is drawn in no such a consideration. From this example it is found that the corrected theoretical curve considerably approaches to the experimental data. Another most cases in our rotary-saturation experiments have a similar

tendency. However, in order to explain our experimental results it is not sufficient to consider only these distributions. Such a discrepancy may be caused by another physical reasons.

References

1) A.G. Redfield: Phys. Rev. **98** (1955) 1787.
2) H. Salwen: Phys. Rev. **99** (1955) 1274.
3) M.N. Hack: Phys. Rev. **104** (1956) 84.
4) S. Wilking: Z. Physik **173** (1963) 490.
5) J.R. Franz and C.P. Slichter: Phys. Rev. **148** (1966) 287.
6) Y. Manmoto, K. Utsunomiya and M. Satoh: J. Phys. Soc. Jpn. **43** (1977) 703.